

Effect of a short region of high convex curvature on heat transfer through a turbulent boundary layer

M. M. Gibson and K. Servat-Djoo

Department of Mechanical Engineering, Imperial College of Science and Technology,
Exhibition Road, London SW7 2BX, UK

Received 13 August 1987 and accepted for publication on 11 July 1988

Extensive surface and single-point turbulence measurements have been made in the turbulent boundary layer on a heated flat surface downstream of a short convex bend with a turning angle of 30° . The purposes of the work were to investigate the response of the temperature boundary layer to an "impulse" of curvature, to discover whether this differs from the response of the velocity boundary layer, and to provide measurements of both in enough detail to be of use to turbulence modelers. One effect of the attenuation of turbulence in the bend is to reduce the Stanton number for surface heat transfer to 82% of the value it would otherwise have had in flat-wall flow. A substantially larger fall in the skin-friction coefficient is attributable to pressure-gradient effects. The results can be interpreted in the light of a postulated damped oscillatory response to the perturbation. In these terms it is found that the period and amplitude of the temperature flux and variance are greater than the period and amplitude of the shear stress and intensity. The results do not support the view that heat transfer is more sensitive than momentum transfer to curvature effects, but there is some indication that the effects of very strong curvature may differ quantitatively from the effects of prolonged mild curvature observed in earlier experiments.

Keywords: turbulent boundary layer; convective heat transfer; streamline curvature; turbulence

Introduction

The effects of complex strains and body forces on heat transfer in turbulent flow are important to engineers who need to predict temperatures and heat-transfer rates on curved and rotating surfaces in turbomachines and similar devices. Though there have been several valuable investigations into the effects of streamline curvature on shear-layer turbulence, comparatively little has been done to quantify the behavior of the thermal turbulence in heated flows of this type. Qualitatively the behavior of the temperature flux will be much the same as that of the shear stress, and in calculation methods it may be accounted for approximately by some suitable form of Reynolds analogy. There is, however, some experimental evidence,¹⁻⁴ which is supported by theoretical considerations,^{5,6} to suggest that heat transfer and momentum transfer are not affected equally by changes in wall curvature, and that the differences are significant enough to warrant further study. The experiment to be described is the latest in a series which have as their chief objective the provision of data on this topic for the further development of calculation methods.

Previous investigations have dealt with the effects of wall curvature sufficiently prolonged for the turbulence to reach some new near-equilibrium state. Thus in a mildly curved convex wall flow,¹ where the radius of curvature R was nominally 100 times the boundary-layer thickness δ , the skin-friction coefficient and the Stanton number were reduced to 88% and 82% of estimated flat-wall values when the flow had proceeded for a distance equal to 50δ . Changes in the corresponding concave-wall flow² were 112% and 119%, respectively. Further evidence of the apparent greater sensitivity of heat

transfer to the effect of wall curvature is provided by the measurements of Simon *et al.*^{3,4} In these experiments the curvature of the convex wall was sufficiently large ($\delta/R=0.1$) and sufficiently prolonged ($x=17\delta$) for c_f and St to fall to about two thirds of estimated flat-wall values. The relative reduction in St was slightly greater than the reduction in c_f , and the eddy-diffusivity ratio (turbulent Prandtl number), determined from profile laws for the inner layer, showed an increase of about 50% in the curved flow. A noteworthy feature of these experiments was that the rate of recovery of c_f and St to self-preserving flat-wall values downstream was unexpectedly slow.

The present investigation is directed at the recovery from curved flow to flat. The experiment is a further development of the response of a boundary layer to an "impulse" of wall curvature described by Smits *et al.*⁷ (hereafter cited as SYB). A developed boundary layer on a flat wall is turned through 30° on a short convex bend 3δ in length with $\delta/R=0.17$. The SYB measurements were made in an isothermal flow; in the present experiment the test wall was heated to a nominal 15 K above the temperature of the free stream. Velocity-field data like those of SYB are now supplemented by measurements of surface heat transfer and velocity-temperature correlations in the flow. The SYB results revealed behavior like that of a second-order system with subcritical damping. The shear stress and intensity recovered quickly in the flow downstream of the bend and, in the outer layer, rose above the levels found at the bend entry, although c_f and the structural parameters appeared to return monotonically to the undisturbed values.

The response of a temperature boundary layer to this type of impulse curvature may be expected to differ in a number of

ways. First, the effects of pressure gradients in the bend will ensure that the initial changes in c_f and St will be different. Intuition suggests, and calculations⁸ confirm, that some of the reduction in c_f at the bend exit is attributable to the deceleration of the inner layer on passing from a curved to a flat wall. Second, there is no reason to suppose that the structural changes produced by streamline curvature in the temperature and velocity outer layers will be exactly the same, and, third, the recovery rates may be expected to be different because the thermal and mechanical time scales are unequal. Like SYB we expect the step response of the system to help to illuminate the steady-state behavior.

The paper contains the results of measurements of surface heat fluxes, the four nonzero components of Reynolds stress and triple velocity products and, in the temperature boundary layer, measurements of the mean-square temperature distributions, temperature fluxes and triple velocity-temperature products.

Apparatus and experimental techniques

The test boundary layer was formed in the working section of the conventional open-circuit blower wind tunnel used in previous experiments^{1,2} which is now fitted with a new contraction and working sections of 5.6 aspect ratio. The working

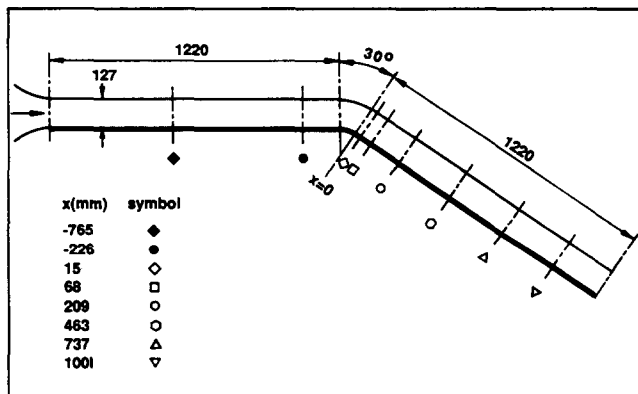


Figure 1 Wind-tunnel working section showing location of the convex bend, traverse positions and symbols. Dimensions in mm

section geometry shown in Figure 1 is similar to that of the 30° convex bend described by SYB, which had an aspect ratio of 6. The boundary layer was tripped at exit from the tunnel contraction and then developed naturally over a distance of 1.22 m on the floor of a 711 × 127 mm² constant-section straight duct to a thickness $\delta = 22$ mm at the start of the bend section. The bend section itself was fabricated from a 30° segment of an aluminum pipe of outside radius $R = 115$ mm machined to a smooth finish. The SYB bend was of 127 mm radius. The distorted boundary layer at the bend exit recovered to normal plane-wall conditions on the heated flat floor of a second 1.22-m-long duct fitted downstream.

Traverse measurements were taken at the streamwise positions shown in Table 1 and Figure 1. Mean-velocity measurements were made by flattened stagnation tubes (using the static pressure at the wall) and by constant-temperature hot-wire probes. Over most of the recovery flow the differences in mean velocity obtained by the two methods differed by less than 1%. At $x = 15$ mm, differences of order 3% reflected the presence of transverse pressure gradients which also affected the momentum balance in this region close to the bend. The shear stress at the surface was obtained in three ways: (a) by the conventional Clauser method of fitting measured velocity profiles to an assumed universal law of the wall:

$$u^+ = 1/K \ln(y^+) + C \quad (1)$$

with $K = 0.41$, $C = 5.0$, (b) by the use of Preston tubes and, (c) by the use of sublayer probes (Stanton tubes) each made from a small piece of razor blade fastened over a static hole. The razor blade method is described by Pai and Whitelaw⁹; its application in a convex wall flow is described by Okamoto and Gibson.¹⁰

The pressure distribution measured at surface tappings and the corresponding changes in free stream velocity are plotted in Figure 2, and details of the mean flow development are summarized in Table 1. The reference velocity was held at 28.5 m/s throughout the experiments. It is the velocity of the free stream at the first measurement position, $x = -765$ mm, measured along the surface from an origin at the bend exit. δ and Δ are defined as the distances from the wall to the points where the local mean velocity and temperature are $0.995U_e$ and $0.995(T_w - T_e)$. Figure 2 shows that the bend produced a significant fall in wall pressure upstream and a corresponding adverse gradient on the recovery plate. The pressure-gradient

Notation

| | |
|-------|---|
| C | Constant in velocity wall law Equation 1, value 5.0 |
| C' | Constant in temperature wall law Equation 4, value 3.0 |
| c_f | Skin-friction coefficient |
| H | Boundary-layer shape factor δ_1/δ_2 |
| K | Constant in velocity wall law Equation 1, value 0.41 |
| K' | Constant in temperature wall law Equation 4, value 0.45 |
| K_a | Acceleration parameter |
| Pr | Prandtl number |
| q | Temperature flux $\bar{v}\theta$ |
| q^2 | $\overline{u'^2 + v'^2 + w'^2}$ |
| R | Surface radius of curvature |
| Re | Reynolds number |
| St | Stanton number |
| T | Mean temperature |
| T^+ | Dimensionless temperature $u_\tau(T_w - T)/q_w$ |
| U | Component of mean velocity parallel to the surface |

| | |
|----------------------|--|
| u, v, w | Components of the fluctuating part of the velocity |
| u_τ | Shear velocity $\sqrt{\tau_w/\rho}$ |
| u^+ | Dimensionless velocity U/u_τ |
| x, y | Coordinates along and normal to the surface |
| <i>Greek symbols</i> | |
| δ | Boundary-layer thickness |
| δ_1 | Boundary-layer displacement thickness |
| δ_2 | Boundary-layer momentum thickness |
| Δ | Temperature boundary-layer thickness |
| Δ_2 | Temperature boundary-layer integral thickness |
| ε | Dissipation rate of $q^2/2$ |
| ε_θ | Dissipation rate of $\theta^2/2$ |
| θ | Fluctuating part of the temperature |
| ρ | Density |
| τ | Shear stress |
| <i>Subscripts</i> | |
| e | Boundary-layer edge conditions |
| ref | Reference conditions |
| w | Wall conditions |

Table 1 Details of the mean flow and list of symbols

| x (mm) | Symbol | U_w/U_{ref} | δ (mm) | δ_1 (mm) | δ_2 (mm) | Δ (mm) | Δ_2 (mm) | (a) | $c_f \times 10^3$ (b) | (c) | $St \times 10^3$ |
|-------------|--------|---------------|------------------|--------------------|--------------------|------------------|--------------------|------|--------------------------|-------------------|------------------|
| -765 | — | 1.000 | 12.5 | 1.83 | 1.29 | 15.3 | 1.57 | 3.50 | — | — | 2.09 |
| -560 | — | 1.006 | 15.3 | 2.29 | 1.64 | 18.3 | 1.85 | 3.30 | — | — | 1.97 |
| -308 | — | 1.020 | 20.4 | 2.95 | 2.14 | 21.0 | 2.37 | 3.14 | — | — | 1.82 |
| -226 | ● | 1.027 | 20.8 | 3.19 | 2.31 | 21.4 | 2.47 | 3.04 | — | — | 1.78 |
| 15 | ◇ | 1.168 | 22.0 | 2.96 | 2.06 | 22.0 | 2.73 | — | 1.85 | — | 1.57 |
| 68 | □ | 1.090 | 24.3 | 3.92 | 2.63 | 23.0 | 2.72 | 1.95 | 1.91 | 1.75* | 1.45 |
| 209 | ○ | 1.057 | 24.8 | 4.26 | 2.87 | 26.1 | 3.18 | 2.31 | 2.23 | 2.12 | 1.44 |
| 467 | ○ | 1.061 | 26.0 | 4.37 | 3.07 | 27.1 | 3.39 | 2.60 | 2.50 | 2.38 | 1.48 |
| 743 | △ | 1.073 | 28.6 | 4.74 | 3.40 | 29.2 | 3.98 | 2.67 | 2.66 | 2.75 ⁺ | 1.50 |
| 1001 | ▽ | 1.077 | 31.9 | 4.98 | 3.64 | 31.2 | 4.37 | 2.74 | 2.75 | — | 1.53 |

c_f measurements (a) by Clauser method, (b) by Preston tube, (c) by sublayer tube (razor blade), * at $x=40$ mm, ⁺ at $x=860$ mm. $U_{ref}=28.5$ m/s

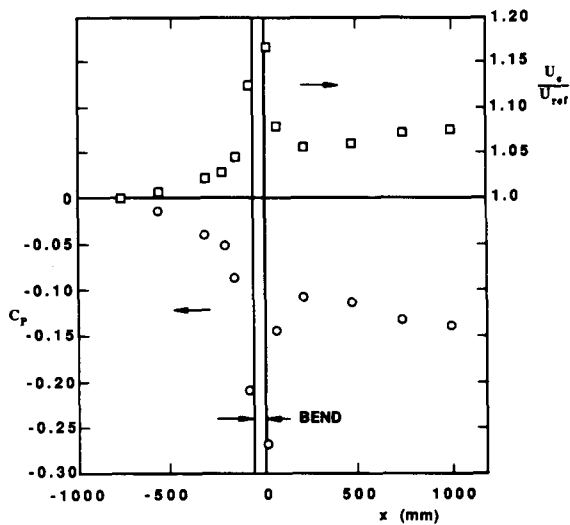


Figure 2 Streamwise variation of the static pressure coefficient $c_p = 2(p - p_{ref})/\rho U_{ref}^2$, and the corresponding variation of U_w/U_{ref}

parameter $(\delta_1/\tau_w)(dp/dx)$ at $x = -226$ mm was approximately -0.24 . (SYB estimated -0.05 at their first measurement station, $x = -185$ mm.) In the downstream recovery flow, far from the bend, the value of this parameter was -0.08 , and the free stream velocity at the last measurement station at $x = 1$ m was $1.077U_{ref} = 30.7 \text{ m} \cdot \text{s}^{-1}$. The skin-friction coefficient before the bend was slightly lower than the value of 0.00317 expected for a constant-pressure flow at a momentum-thickness Reynolds number of 4500 .

Surface flow visualization by liquid film on the recovery plate showed flow from the corners to the centerline resulting from the inward motion of the end-wall boundary layers in the bend. The effects were, however, confined to the corner regions, and for a span of at least 200 mm in the center of the plate the flow appeared to be sensibly parallel. Spanwise measurements in the boundary layer and on the surface with Preston tubes also confirmed this finding. For the recovery flow the centerline values of c_f shown in Table 1 agree well with values estimated from the two-dimensional integral momentum equation for $x > 200$ mm, where the pressure-gradient contribution fell gradually from 35 to 25% of $d\delta_2/dx$. The imbalance appears to be of the same order as that found by SYB. The momentum-balance values lie up to 14% above the measured values, presumably on account of slight convergence of the mean flow streamlines. The maximum discrepancy occurred at $x = 300$ mm, but improved with distance from the bend until far downstream the measured and balance values nearly coincide. The integral

momentum equation was not, however, satisfied in the immediate vicinity of the bend ($x < 200$ mm), not necessarily on account of three-dimensional effects but more probably because the two-dimensional equation is both sensitive to strong pressure gradients and does not allow for the presence of transverse pressure variation.

The tunnel floors were made of 12.5 -mm aluminum plate and, with the bend, were heated by electric blankets to a mean temperature nominally 14.6 K above that of the free stream. The variation in surface temperature measured by copper-constantan thermocouples embedded in the plates and in the surface of the bend nowhere exceeded ± 0.75 K from the mean. The temperature differences in the flow were small enough for the temperature to be considered to be a passive scalar and, as in our previous work,^{1,2} buoyancy effects were negligibly small. Surface heat-transfer measurements were made, as before, with interchangeable 9.4 -mm-diameter heat-flux meters of the Schmidt-Boelter multiple-thermocouple type. These meters have linear characteristics with a sensitivity of 40 mV/W/cm^2 , and in these experiments an output of about 5 mV , which was measured on a Datron 1065A digital voltmeter. Heat-flux measurements on the plates were repeatable with different meters to within 2.5% . Mean temperatures in the flow were measured with a $12 \mu\text{m}$ diameter Chromel-Alumel thermocouple sensor welded to a standard miniature hot-wire probe. The fluid properties used in data reduction were evaluated at the film temperature, $0.5(T_w + T_e)$. Downstream of the bend the growth of Δ_2 was nearly linear and corresponded to a constant Stanton number of approximately 0.0015 , in close agreement with the values of St in Table 1.

The techniques employed for turbulence measurements have been described in some detail in previous papers,^{1,2} and in the thesis by Verriopoulos.¹¹ Only a short account is needed here. Velocity measurements were made using 1 -mm-long, 5 - μm -diameter hot wires fitted to miniature probes in a dual-channel DISA 55M01 constant-temperature anemometer. The hot-wire signals were linearized and processed¹¹ in an on-line micro-computer system. Mean-square temperature fluctuations and temperature-velocity correlations were obtained from measurements with a three-wire probe in which a 1.25 - μm , 50 - Ω , cold resistance-thermometer wire, 1 mm long, operated at a resistance overheat ratio of 1.001 , was positioned in the plane midway between hot wires separated by 1.2 mm in a standard DISA 55P61 X-probe. The measurement volume was approximately 1.2 mm^3 . The cold-wire signal was compensated digitally as described by Verriopoulos.¹¹ Check measurements of $\overline{u^2}$, $\overline{u\theta}$, and $\overline{\theta^2}$ from a parallel twin (hot+cold) wire probe agreed to within $\pm 3\%$ of the three-wire results. The measurements to be described and discussed in the following sections were taken mainly in the downstream recovery flow.

Results

The mean flow

The main features of the flow are evident in the results of mean-velocity, temperature and surface measurements which are summarized in Table 1, and the variation of shape factor, skin-friction coefficient, and Stanton number shown in Figure 3. The heated boundary layer developed initially in a mild favorable pressure gradient on the upstream half of the preplate. From $x = -500$ mm, however, it was gradually accelerated to the bend entry (Figure 2) where its thickness was 22 mm. The momentum thickness Reynolds number at this point was 5225, and the thickness of the temperature boundary layer 24 mm. The streamwise changes in c_f and St upstream of the bend are tolerably well fitted in Figure 3 by conventional power laws:

$$c_f = 0.0592 Re_x^{-0.2} \tag{2}$$

$$St = 0.0296 Pr^{-0.4} Re_x^{-0.2} = 0.5c_f Pr^{-0.4} \tag{3}$$

when a virtual origin is taken at $x = -1.5$ m. The boundary layers emerging from the bend were reduced in thickness and distorted by the effects of pressure gradient and the extra strains associated with the longitudinal curvature. In the latter part of the bend these two effects combined to produce velocity profiles characteristic of deceleration (in the inner layer) and stabilizing curvature (in the outer layer), with low values of c_f and high values of the shape factor H , which was increased in the bend as is usual in convex-wall flow.¹ The subsequent steep increase just downstream of the bend was the response to increasing pressure in this region, not shown by SYB because they did not take measurements close to the bend, but entirely consistent with the results of calculations of their flow.⁸ H , c_f , and St

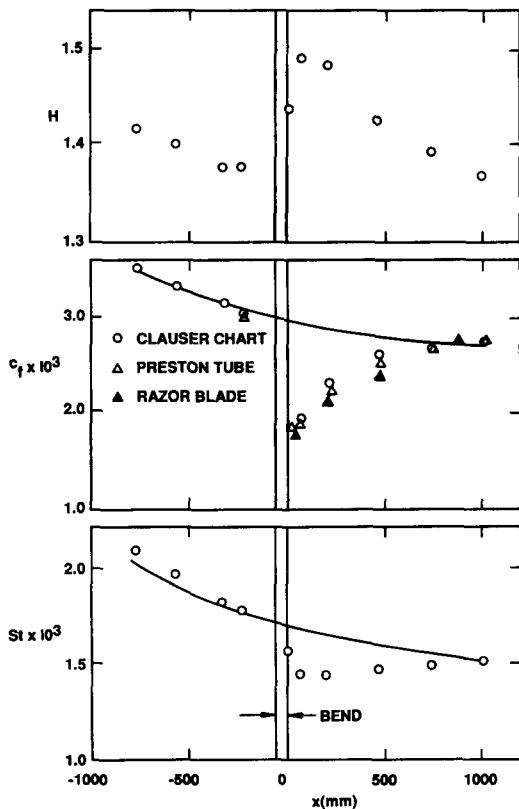


Figure 3 Variation of boundary-layer shape factor, skin-friction coefficient and Stanton number. Lines are flat-plate correlations, Equations (2) and (3)

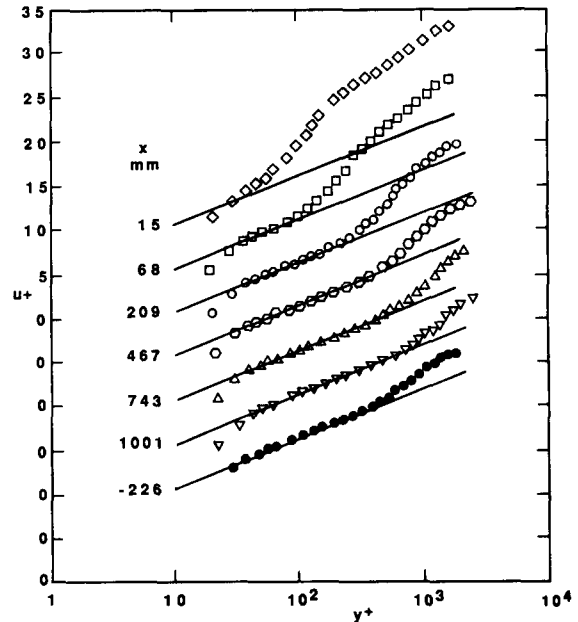


Figure 4 Mean-velocity profiles in inner-layer coordinates. Lines from the wall law (1) with $K=0.41$, $C=5.0$

subsequently approached typical flat-wall values monotonically some 50 boundary thicknesses downstream.

The velocity profile at $x = 15$ mm, plotted in wall coordinates in Figure 4, shows the departure from the law of the wall typical of a boundary layer in a strong adverse pressure gradient which precludes the use of the Clauser method for skin friction. In reducing the data the Preston tube value has been used for this point; elsewhere reliance is placed on the Clauser chart values, which differ only slightly from the Preston tube measurements. Both methods are based on the assumption of a universal velocity distribution in the (turbulent) inner layer. Note that, in order to keep Figure 4 reasonably compact, the profile upstream of the bend, which is distinguished by filled symbols, is plotted below those from the recovery flow downstream. It may also be noted from Table 1 that lower values of c_f are consistently obtained from the sublayer probes in the downstream flow. This finding supports a view¹² that the Clauser method tends to underestimate changes in c_f due to wall curvature because the universal law of the (flat) wall does not allow for effects of structural changes in curved-wall boundary layers.

Figure 3 shows changes in the Stanton number which differ from those in c_f , mainly because of the absence of direct effects of the pressure gradient on the temperature layer. Thus while the minimum value of c_f is about 60% of the value given by Equation 2 at the bend exit, the fall in St is only to about 82% of the corresponding value given by Equation 3. This happens also to be the change in St obtained previously¹ in a distance of 50δ on a long mildly curved bend. Unlike c_f , St also apparently continues to decrease on the flat plate to a shallow minimum at about 5δ from the bend exit. Mean-temperature profiles in the recovery flow are plotted in wall coordinates in Figure 5, where they are compared with the inner law

$$T^+ = 1/K' \ln(y^+) + C' \tag{4}$$

with $K'=0.45$, $C'=3.0$.¹² In marked contrast to the results of our earlier work,¹ and to those of Simon and Moffat,³ the gradients in the inner layer are apparently unchanged from flat-wall flow, even in the first two profiles where the departure from Equation 4 is large. Thus the value of the ratio K/K' , which may be regarded as a sort of global eddy-diffusivity ratio,

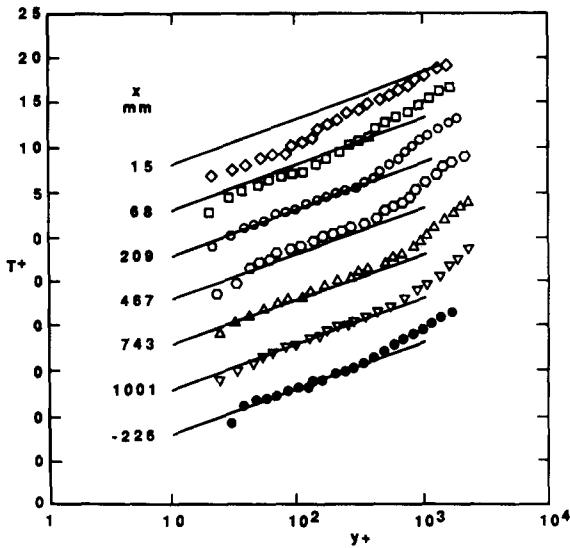


Figure 5 Mean-temperature profiles in inner-layer coordinates. Lines from the wall law (4) with $K' = 0.45$, $C' = 3.0$

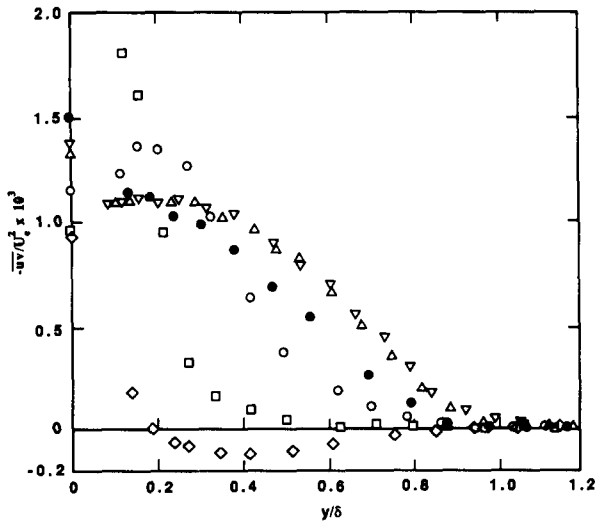


Figure 6 Profiles of the shear stress, $-\overline{uv}$. Values at the wall from Table 1 are plotted on the ordinate. Symbols as in Figure 1 and Table 1

or turbulent Prandtl number for the inner layer, is approximately constant and equal to 0.91 for $K = 0.41$, $K' = 0.45$. The poor fit to Equation 4 of the profiles close to the bend is due to the influence of the adverse pressure gradient on the wall shear which results in lower values of T^+ than would be obtained in a constant-pressure flow.

Second-order turbulence correlations

The response of the shear stress to the conditions in the bend, and the recovery downstream, is essentially as described by SYB, and changes in the profiles shown in Figure 6 do not differ significantly from those of their experiment. In the immediate vicinity of the wall the limited spatial resolution of the X-probe results in shear stress values that are about 12% low. For $y/\delta < 0.2$, the distance from the wall and the scale of the energy-containing eddies are of the same order as the wire lengths and separation distance. Inability to resolve the motion at smaller scales is critical in this region, where the Kolmogorov

scale ranges from approximately 0.03 to 0.05 mm. The resolution necessarily improves with distance from the wall as the energy spectrum widens, the integral scale increases as y , and the Kolmogorov scale as $y^{1/4}$, and it is in the outer layers that the distorting effects of the bend are most apparent. The effects of local turbulence intensity tend further to depress the near-wall measurements by about 3%. The measurements were repeatable to within $\pm 5\%$.

The profile closest to the bend exit shows the effect of strong stabilizing curvature on the structure of the outer layer, where the shear stress is reversed in direction for $y > 0.2\delta$. The changes in the outer layer influence conditions in the inner layer, and hence the wall shear, through the shear-stress gradient. The inner-layer distribution at this position exhibits a steep negative gradient with some hint of a maximum very close to the wall that would be consistent with a history of inner-layer deceleration. Such a maximum is seen in the second profile at a point where the recovery process is well under way. The sequence of events is described by SYB. As the flow proceeds downstream, the turbulence intensity and shear stress in the outer layer increase, and typical values of $\partial U/\partial y$ in the inner layer decrease, toward the self-preserving state. A combination of high values of $\partial U/\partial y$ and of turbulent transport from below then causes turbulence

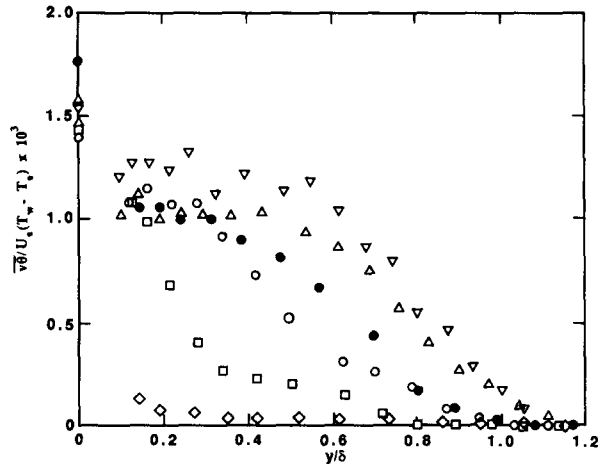


Figure 7 Profiles of the cross-stream temperature flux, $\overline{v\theta}$. Values at the wall from Table 1 are plotted on the ordinate. Symbols as in Figure 1 and Table 1

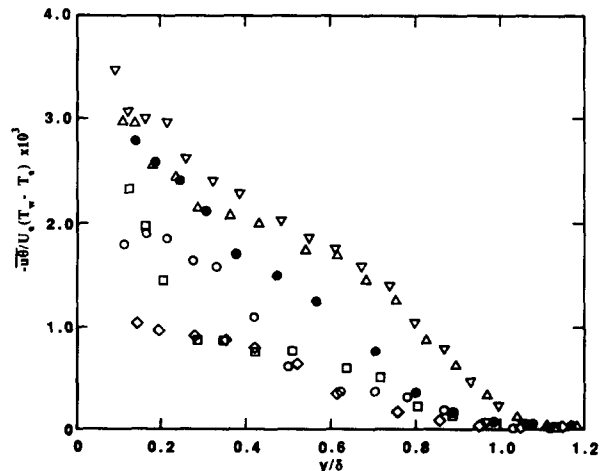


Figure 8 Profiles of the streamwise temperature flux, $-\overline{u\theta}$. Symbols as in Figure 1 and Table 1

quantities in the outer layer to rise above flat-wall levels. Figure 6 shows the way in which the peak in shear stress near $y/\delta=0.1$ propagates outward as a stress wave exactly as found by SYB. The distribution at the last two downstream stations are nearly coincident but remain above that of the plane approach flow in the outer layer. The final approach to conditions in an ordinary flat-wall boundary layer appears likely to be slow.

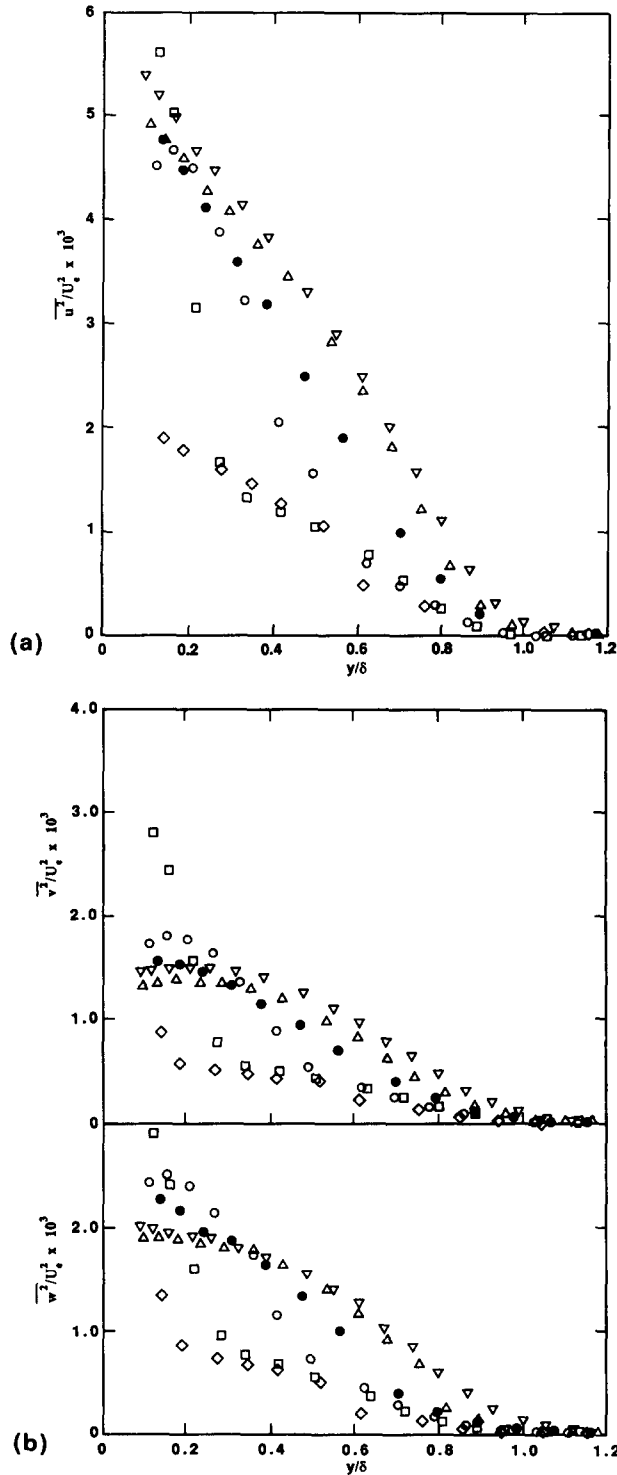


Figure 9 (a) Profiles of the normal stress $\overline{u^2}$. Symbols as in Figure 1 and Table 1; (b) profiles of the normal stresses $\overline{v^2}$ and $\overline{w^2}$. Symbols as in Figure 1 and Table 1

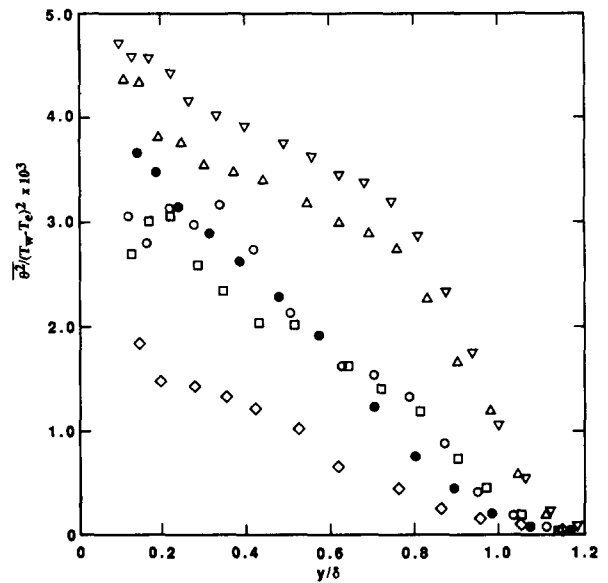


Figure 10 Profiles of the temperature variance. Symbols as in Figure 1 and Table 1

Profiles of the two temperature fluxes are plotted in Figures 7 and 8. The $v\theta$ measurements, like those of the shear stress, show the effects of the limited spatial resolution possible with the three-wire probe. For $y/\delta < 0.2$, the probe measurement volume of 1.2 mm^2 was of the same order as the distance from the wall, and of the larger turbulent scales, and 20–30 times the Kolmogorov temperature scale. The longitudinal flux $-\overline{u\theta}$ is believed to have been less sensitive, and the two- and three-wire probes gave results in agreement to within $\pm 3\%$. The attenuation of $\overline{v\theta}$ close to the wall is greater because more significant contributions to v' and θ' are made by motion at the smaller scales. Figure 6 shows that the probable discrepancy near the wall is greater than that in $-\overline{uv}$ and may exceed 15% at $y=0.14\delta$ in the thin boundary layer upstream of the bend. As with the shear stress, the spatial resolution improves as the distance from the wall increases and, to a lesser extent, as the boundary layer thickens in the recovery flow downstream of the bend. The measurements were repeatable to within $\pm 5\%$.

The behavior of the temperature flux is not dissimilar to that of the shear stress, but it is less spectacular. Figure 7 shows that, while $\overline{v\theta}$ is close to zero in the outer 80% of the layer, there is no sign reversal implying up-gradient diffusion. Since there is no equivalent to the shear-stress peak in the inner layer the changes in that region are relatively small. But in the outer layer the recovery to, and overshoot of, self-preserving values is of the same order as in the shear stress. Figure 8 shows profiles of the streamwise flux $-\overline{u\theta}$. This quantity is, as expected,¹ approximately $-2\overline{v\theta}$ in the upstream boundary layer. It exhibits very much the same sort of recovery behavior, from minimum values of about one third of the approach flow levels.

The recovery of the turbulent energy components is similar to that of the shear stress, and clearly shows changes consistent with the passage of a stress wave as conjectured by SYB. The profiles plotted in Figure 9 also show that the attenuation and rate of recovery are approximately the same in all components. The relative weighting of the component energy production terms is of little consequence in highly curved flow when the shear stress is zero. The measurements in Figure 10 show that the mean-square temperature fluctuations respond more quickly.

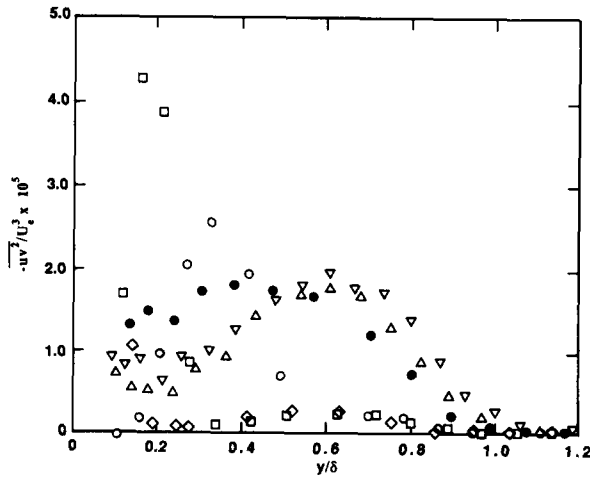


Figure 11 Profiles of the triple velocity correlation $\overline{uv^2}$ associated with shear-stress transport. Symbols as in Figure 1 and Table 1

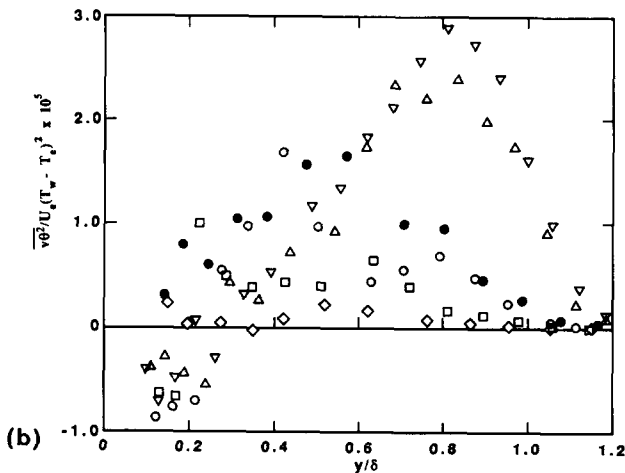
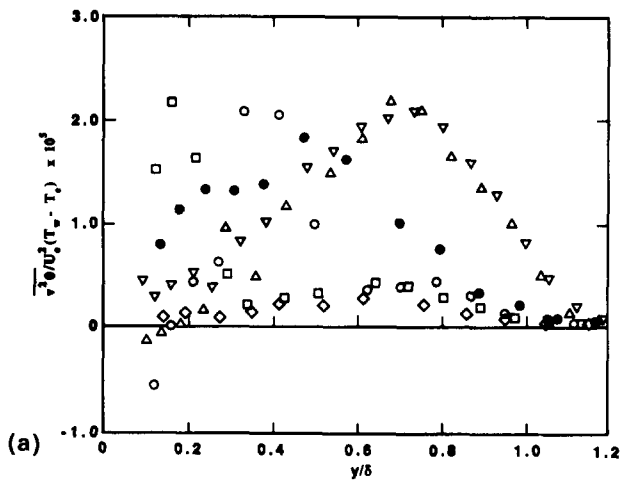


Figure 12 (a) Profiles of the triple velocity-temperature correlation $\overline{v^2\theta}$ associated with the cross-stream transport of $v\theta$. Symbols as in Figure 1 and Table 1; (b) profiles of the triple velocity-temperature correlation $\overline{v\theta^2}$ associated with cross-stream transport of θ^2 . Symbols as in Figure 1 and Table 1

At the bend exit the level has been reduced to about half of that of the upstream flow, on account of the reduction in $v\theta$ in the production rate of θ^2 . At the second position, three boundary-layer thicknesses downstream, the upstream levels have effectively been reached, while at the end of the recovery flow, 1 m from the bend, values in the outer layer are more than twice those of the approach flow. Moreover, while the distributions of the other second moments at the last two positions nearly coincide, suggesting the beginning of a slow return to self-preserving values from above, the profiles of θ^2 show a continuing increase in this quantity.

The triple products

Turbulent diffusion of the second moments is dominated by the large-scale motion which is most sensitive to changes in curvature. This sensitivity is reflected in very substantial changes in the distributions of uv^2 , which are shown in Figure 11, and in the distributions of the other triple velocity products presented by Servat-Djoo¹³ but omitted here for conciseness. At the exit from the bend the turbulent diffusion of stress and intensity is almost entirely suppressed in the outer layer. Peaks similar to and associated with those in the shear stress and intensity appear first very close to the wall, far in excess of the normal flat-wall values. These peaks quickly propagate outward, diminishing in size until, by the last downstream positions where they have reached the outer layer, they are only fractionally above the self-preserving levels. In the inner layer the distributions lie below the flat-wall profile and they possess slopes large enough to suggest that turbulent diffusion is not insignificant in this region. SYB provide a detailed discussion of similar results which it is unnecessary to repeat here.

The same general behavior is shown in the distributions of the triple velocity-temperature product which are plotted in Figure 12. Here, however, the last profiles far downstream are very different from the flat-wall profiles, with peaks at $y=0.8\delta$ over twice as great as the flat-wall values, and much lower values in the inner layer. As in earlier convex-wall experiments,¹ the appearance of negative values of $\overline{v\theta^2}$ in the inner layer implies inward diffusion of θ^2 in this region.

Discussion and conclusion

The reduction in the surface heat flux, which appears small in relation to the fall in skin friction, may be assessed in the light of the results obtained by Simon *et al.*^{3,4} from the heated flow on a prolonged bend. The nominal strength of the curvature δ/R was less than in the present case (0.1 compared to 0.15), and the pressure gradients were smaller but at 32° of turn, six boundary-layer thicknesses in the bend (3.3 in the present case), conditions appear to be roughly comparable. The shear stress was reversed over most of the outer layer, as in the bend-exit distribution of Figure 6, and a dimensionless stress gradient $\delta\tau^+/\delta y^+$ of about -0.003 in the inner layer compares with the present value of about -0.005 . At this point the reduction in Stanton number was almost exactly the same as in the present experiment: to 80% of the estimated flat-wall value (Figure 3). The two sets of data thus appear to be reasonably consistent in this respect. In the present case the extra strain of the bend flow is applied briefly and the Stanton number still has two thirds of the way to fall to a new value estimated roughly to be 40% of that on a flat wall, and there are the additional complications associated with the presence of significant pressure gradients in and near to the bend.

The minimum Stanton number does not occur for another ten boundary-layer thicknesses downstream, in contrast to the quick recovery of the skin friction coefficient from a much lower level. The behavior of c_f is, however, naturally sensitive to the pressure gradients which would appear not to have much effect on St. A rough calculation shows maximum values (+ or -) of the acceleration parameter $K_a = (v/U_c^2)(\partial U_c/\partial x)$ to be about 0.2×10^{-6} , which, according to Kays correlation,¹⁴ are not enough to cause St to vary by more than 2%. The effect of the pressure gradients on the skin friction are far from negligible. These values of K_a imply that in the integral momentum balance, the contribution to c_f from this source may be up to three times that of the momentum-thickness gradient. An initial acceleration of the inner layer produces a sharp rise in c_f and tends to augment the effect of curvature in the outer layer by producing the steep negative stress gradient shown in Figure 6. In the decelerated inner flow at the bend exit the surface stress is reduced, and the stress gradient in the inner layer is positive; $\partial(-\overline{uv})/\partial y = \partial p/\partial x$ approximately. At the same time, however, the effect of the curvature is to reverse the direction of the shear stress in the outer layer. The two effects combine to produce a stress distribution with a maximum very close to the wall which forms the springboard for the subsequent quick recovery and the "stress wave" described by SYB.

At the exit from the bend $\overline{v\theta}$ is effectively zero in the outer 80% of the layer. It, like the shear stress, is regenerated from the wall outward, but the distributions have no visible peaks and the flux gradient in the inner layer is negative. This gradient cannot be sustained when the curvature effects are suddenly removed, and, since the rate of recovery in the outer layer is finite and it takes some time to affect conditions at the wall, the first step in the recovery flow is a further fall in the wall flux. In short, at the bend exit the wall shear is less than the maximum in the inner layer so that when the wall conditions change it will tend to increase. Conversely, the surface heat flux is greater than the inner-layer values and the first response to the removal of the curvature is a further decrease, before increasing turbulence production brings about a final gradual increase to flat-wall levels.

The inner layer is not, however, the place to compare the relative rates of recovery of the distorted velocity and temperature fields. It is in the outer layer that the direct effects of additional strains are felt and the complications of the streamwise pressure gradient are relatively slight. In this region the shear-stress and intensity measurements support SYB's hypothesis that the response is a damped oscillatory variation but one in which both the period and the amplitude of the $v\theta$ oscillation are probably substantially greater than the period and amplitude of the \overline{uv} oscillation, possibly by a factor of about 2. Thus at a representative point in the outer layer, $y/\delta = 0.6$, the maximum shear stress and intensities occur at about $x = 900$ mm, while $\overline{v\theta}$ and the mean-square temperature fluctuations are still rising at the end of the plate. This unexpected result is at variance with earlier tentative conclusions¹ that thermal turbulence is not only more sensitive to curvature effects but that the response to a perturbation is more rapid. Here the sensitivity is seen, not in the virtual suppression of the temperature flux in the outer layer of the bend flow, which is less extensive than that of the shear stress, but in the greater amplitude of the damped oscillation downstream.

A primary objective has been to provide heat-transfer data for turbulence modelers. The effects of wall curvature generally, and the response to an impulse of curvature specifically, cannot be predicted properly by mean-field closure methods employing simple expressions for an eddy viscosity, and that second-

moment closures at least will be needed—i.e., the solution of modeled equations for the Reynolds stresses and temperature fluxes. A Reynolds stress model does give good results for the isothermal SYB flow^{8,15} and faithfully reproduces the distortion in the bend and the slow recovery downstream. Heat-transfer calculations are more difficult, partly because the problem of modeling equations for the temperature fluxes has received comparatively little attention, but also because analyses like that in Ref. 5 for various modeled equations produce theoretical results at variance with existing measurements.¹⁻³ It is disappointing that the best that can be done now is to relate the temperature fluxes to the Reynolds stresses through an assumed turbulent Prandtl number distribution. Meanwhile the results of the present experiment augment the small database available to modelers.

Acknowledgment

The authors gratefully acknowledge financial support for this research which has been provided by Grant No. GR/C19653 from the Science and Engineering Research Council.

References

- Gibson, M. M. and Verriopoulos, C. A. Turbulent boundary layer on a mildly curved convex surface. Part 2: Temperature field measurements. *Expts. Fluids*, 1984, **2**, 73-80
- Gibson, M. M. and Servat-Djoo, K. Measurements in the heated turbulent boundary layer on a mildly curved concave surface. *Proc. 5th Turbulent Shear Flows Symp.*, Cornell University, 1985
- Simon, T. W. and Moffat, R. J. Heat transfer through turbulent boundary layers—the effects of introduction of and recovery from convex curvature. ASME Paper No. 79-WA/GT-10, 1979
- Simon, T. W., Moffat, R. J., Johnston, J. P., and Kays, W. M. Turbulent boundary layer heat transfer experiments: convex curvature effects including introduction and recovery. Stanford University Mech. Eng. Report No. HMT-32, 1980
- Gibson, M. M. An algebraic stress and heat-flux model for turbulent shear flow with streamline curvature. *Int. J. Heat Mass Transfer*, 1978, **21**, 1609-1617
- Gibson, M. M. Effects of streamline curvature on turbulence. *Frontiers in Fluid Mechanics*. (eds., Davis, S. H. and Lumley, J. L.), Springer, 1985, pp. 184-198
- Smits, A. J., Young, S. T. P., and Bradshaw, P. The effect of short regions of high surface curvature on turbulent boundary layers. *J. Fluid Mech.*, 1979, **94**, 209-242
- Gibson, M. M., Jones, W. P., and Younis, B. A. Calculation of turbulent boundary layers on curved surfaces. *Phys. Fluids*, 1981, **24**, 386-395
- Pai, B. R. and Whitelaw, J. H. Simplification of the razor blade technique and its application to the measurement of wall shear stress in wall jet flows. *Aero. Q.*, 1969, **XX**, 355-364
- Okamoto, S. and Gibson, M. M. Skin-friction measurements on a convex wall. Imperial College MED Report No. FS/86/12, 1986
- Verriopoulos, C. A. Effects of convex curvature on heat transfer in turbulent flow, PhD Thesis, Imperial College, 1983
- Gibson, M. M. Effects of surface curvature on the law of the wall. *Proc. Zoran Zaric Memorial Seminar on Near-Wall Turbulence*, Dubrovnik, 1988
- Servat-Djoo, K. The effects of surface curvature on heat transfer through a turbulent boundary layer, PhD Thesis, Imperial College, 1987
- Kays, W. M. and Crawford, M. E. *Convective Heat and Mass Transfer*, McGraw-Hill, New York, 1980
- Gibson, M. M. and Younis, B. A. Calculation of swirling jets with a Reynolds stress closure. *Phys. Fluids*, 1986, **29**(1), 38-48